

Dynamics of superconducting pairs in the two-dimensional Hubbard model

G. Sordi,^{1,*} E. M. O’Callaghan,¹ C. Walsh,¹ M. Charlebois,² P. Sémon,³ and A.-M. S. Tremblay³

¹*Department of Physics, Royal Holloway, University of London, Egham, Surrey, UK, TW20 0EX*

²*Département de Biochimie, Chimie, Physique et Science Forensique, Institut de Recherche sur l’Hydrogène, Université du Québec à Trois-Rivières, Trois-Rivières, Québec, Canada, G9A 5H7*

³*Département de physique, Institut quantique & RQMP, Université de Sherbrooke, Sherbrooke, Québec, Canada J1K 2R1*

(Dated: December 2, 2025)

The frequency structure of the superconducting correlations in cuprates gives insights on the pairing mechanism. Here we present an exhaustive study of this problem in the two-dimensional Hubbard model with cellular dynamical mean-field theory. To this end, we systematically quantify the dependence on doping and interaction strength of the superconducting gap, of the frequency scales where pairing occurs, and of their relative contribution to pairing. We find pair-forming alternating with pair-breaking processes as a function of frequency, providing new evidence that pairing can arise in principle from both low- and high-frequency processes. However, we find that the high-frequency pair-forming processes are outweighed by pair-breaking ones. Hence, the net contribution to pairing comes only from the low-frequency pair-forming processes, a result that underscores their key role in the pairing mechanism.

Introduction– The mechanism driving the superconducting pairing of electrons in cuprate superconductors is still under scrutiny [1–3]. It requires knowing how the electrons forming the Cooper pairs are correlated *both* in space and in time. On one hand, the *d*-wave symmetry of the superconducting gap and the short correlation length measured in cuprates suggest that the *spatial dependence* of the pair correlations is nonlocal and short-ranged [3]. On the other hand, the limited experimental information about the *time dependence* of the pair correlations in cuprates [4–8] hinders a thorough characterisation of the pairing mechanism [2, 9].

While first-principle methods now allow material specific predictions [10–14], the detailed information of model calculations can provide valuable insights for clarifying the universal features of the pairing mechanism and for guiding experimental progress. These calculations are even more pressing in view of current proposals for measuring pair correlations with angle-resolved photoemission spectroscopy (ARPES) [15–18]. The strong electron-electron interaction in cuprates indicates that the two-dimensional (2D) Hubbard model, where electrons hop in a square lattice with an amplitude t and experience an onsite Coulomb repulsion U , is the point of departure for modeling the superconducting pairing [2, 19]. However, clarifying the origin of pairing in the Hubbard model is still a theoretical challenge, owing to the nonperturbative nature of the strong electronic correlations [20].

Regarding the *spatial dependence* of the superconducting correlations, the Hubbard model correctly captures their nonlocal character. Physically, this is because the repulsion U (i) disfavors the occurrence of two electrons on the same site and (ii) dynamically generates the antiferromagnetic superexchange interaction $J = 4t^2/U$ which favors antiparallel spins on neighboring sites, and thus their effective attraction [21]. Detailed studies con-

firm these effects brought about by U [2, 20, 22–24].

The issue of the *time dependence*, i.e. of the dynamics, of the superconducting correlations in the Hubbard model has been less explored and is controversial. It is the focus of this work. This is a difficult task, requiring a theory capable to treat on an equal footing different and coexisting time scales, from short time scales associated with the interaction U to longer time scales associated with the superexchange J . Cluster extensions [22, 23, 25] of dynamical mean-field theory [26], which handle both spatial fluctuations (within the cluster) and all temporal fluctuations, provide such a theory.

The key questions concern the characteristic time scales that lead to pairing and their relative contribution to pairing. These features depend on U and doping. Previous studies [27–34] show that the main contribution to pairing arises from relatively long time (low frequency) scales ascribed to short-range spin singlet correlations generated by the superexchange J , with smaller contributions arising from shorter time (higher frequency) scales linked to U . However, these conclusions are drawn from studies on selected range of parameters of the 2D Hubbard model and are based on different methodologies. For example, the pairing dynamics was studied in Ref. [27] with dynamical cluster approximation (DCA) at $U/t = 8, 10, 12$ and 20% of doping at finite temperature T , in Ref. [28] with cellular dynamical mean-field theory (CDMFT) at $U/t = 8$ and few doping levels at $T = 0$, in Refs. [31, 33, 34] with DCA at $U/t = 5.5, 6$ and few doping levels at low T , and in Ref. [32] with CDMFT at $U/t = 9$ and several doping levels at low T .

Here we revisit the problem of the dynamics of the superconducting pairs in the 2D Hubbard model using state of the art calculations based on CDMFT [22, 23, 25] at finite temperature. Methodologically, the added value of our work is twofold. First, taking advantage of algo-

rithmic improvements and large investment of computing time, we explore a dataset encompassing a wide range of interaction U and a comprehensive group of doping levels. Second, our findings are a direct computational result based solely on the Green's function obtained in CDMFT, with no other assumptions coming e.g. from low-frequency theories. Using this approach, we systematically quantify the dependence on doping and U of the characteristic time scales where pairing occurs and their relative contribution to pairing. We find a rich structure in the dynamics of the correlations of the paired electrons, with pair-forming alternating with pair-breaking processes as a function of frequency. Our key finding is that the high frequency pair-forming processes are outweighed by their corresponding pair-breaking processes, so that the net contribution to pairing comes only from the low frequency pair-forming processes.

Model and Method— We study the 2D Hubbard model on the square lattice, $H = -\sum_{ij\sigma} t_{ij} c_{i\sigma}^\dagger c_{j\sigma} + U \sum_i n_{i\uparrow} n_{i\downarrow} - \mu \sum_{i\sigma} n_{i\sigma}$. Here, $c_{i\sigma}$ ($c_{i\sigma}^\dagger$) is the operator that destroys (creates) an electron with spin $\sigma = \{\uparrow, \downarrow\}$ at site i , $n = c_{i\sigma}^\dagger c_{i\sigma}$ is the number operator, t_{ij} is the hopping amplitude between nearest neighbour sites, U is the onsite Coulomb repulsion, and μ is the chemical potential which changes the occupation n and thus the hole doping $\delta = 1 - n$. We set $t_{ij} = t = 1$ as our energy unit.

We solve this model in the $d_{x^2-y^2}$ -wave superconducting state and at finite temperature with CDMFT [22, 23, 25]. CDMFT maps the Hubbard model onto a cluster impurity model embedded in a self-consistent bath of noninteracting electrons. Here we consider the minimal cluster that describes d -wave superconductivity, i.e. a 2×2 plaquette. To solve the cluster impurity model, we use the hybridization expansion continuous-time quantum Monte Carlo method (CT-HYB) [35–37] with a LazySkip List algorithm [38] and with Monte Carlo updates of two pairs of creation and destruction operators to ensure ergodicity [39]. The CT-HYB method enables us to explore the superconducting state for a wide range of interaction strength U and to reach low temperatures.

This work focuses on the dynamics of the superconducting pairs, which is encoded in the Green's function. In the cluster momentum basis, the Green's function is

$$G_{\mathbf{K}}(\tau) = \begin{pmatrix} G_{\mathbf{K}\uparrow}(\tau) & F_{\mathbf{K}}(\tau) \\ F_{\mathbf{K}}^\dagger(\tau) & -G_{-\mathbf{K}\downarrow}(-\tau) \end{pmatrix}, \quad (1)$$

where, introducing the Matsubara frequencies, $G_{\mathbf{K}\sigma}(i\omega_n) = -\int_0^\beta d\tau e^{i\omega_n \tau} \langle T_\tau c_{\mathbf{K}\sigma}(\tau) c_{\mathbf{K}\sigma}^\dagger(0) \rangle$ is the Nambu diagonal (i.e. normal) Green's function and $F_{\mathbf{K}}(i\omega_n) = -\int_0^\beta d\tau e^{i\omega_n \tau} \langle T_\tau c_{\mathbf{K}\uparrow}(\tau) c_{-\mathbf{K}\downarrow}(0) \rangle$ is the Nambu off-diagonal (i.e. anomalous) Green's function. For d -wave superconductivity $F_{\mathbf{K}=(\pi,0)} = -F_{\mathbf{K}=(0,\pi)}$ is the only nonzero component. The superconducting order parameter is $\Phi = \langle F_{\mathbf{K}=(\pi,0)}(\tau = 0^+) \rangle$.

We perform the analytical continuation from imagi-

nary to real frequencies using the maximum entropy software of Ref. [40]. However, for the anomalous Green's function, which shows both positive and negative spectral weight, the application of the direct maximum entropy method is inapplicable. Instead, we use the MaxEntAux method of Ref. [41], which relies on an auxiliary Green's function with positive spectral weight.

Strategy— The strategy of this work is to systematically examine the dependence on doping and U of three key features of the superconducting state: (i) the superconducting gap, (ii) the characteristic frequency scales that contribute to superconducting pairing and (iii) their relative contribution to pairing.

To do that, we first take advantage of previous work that mapped out the superconducting state of the 2D Hubbard model with CDMFT on a 2×2 plaquette in the $U - \delta - T$ space [42–45]. This is condensed in Fig. 1(a), where we report the data of Ref. [42] showing the superconducting transition temperature T_c^{CDMFT} (defined as the temperature below which $|\Phi|$ is nonzero [46]) as a function of δ for different values of U straddling the normal state metal to Mott insulator transition at $U_{\text{MIT}} \approx 5.95$ [47]. Below U_{MIT} (squares), $T_c^{\text{CDMFT}}(\delta)|_U$ reaches its highest value at $\delta = 0$ and monotonically decreases with increasing doping. Above U_{MIT} (circles), $T_c^{\text{CDMFT}}(\delta)|_U$ is zero at $\delta = 0$ and acquires an asymmetric dome-like shape versus δ , reaching its highest value at a finite doping which is dependent on U . As a function of U , T_c^{CDMFT} is optimised just above U_{MIT} (green circles).

Next, we fix the temperature at $T = 1/50$, since it is below the optimum T_c^{CDMFT} for each value of U , and we explore the model for $U \in [5.2, 16]$ and several doping levels. For each value of U and δ we calculate the density of states in the superconducting state $A_{\text{nor}}(\omega) = -\frac{1}{\pi} \text{Im} G_{\mathbf{R}=(0,0)}(\omega)$, the anomalous spectral function $A_{\text{an}}(\omega) = -\frac{1}{\pi} \text{Im} F_{\mathbf{K}=(\pi,0)}(\omega)$, and the cumulative spectral weight of the order parameter [28, 32] $I_F(\omega) = \int_{-\omega}^{\omega} \frac{d\omega'}{2\pi} A_{\text{an}}(\omega') f(-\omega')$. Fig. 1(b),(c),(d) show $A_{\text{nor}}(\omega)$, $A_{\text{an}}(\omega)$ and $I_F(\omega)$ for $U = 12$ and $\delta \approx 0.02$, as a sample of our calculations (see supplemental Figs. S1–S5 for spectra at other model parameters).

From $A_{\text{nor}}(\omega)$, we extract a key feature of the superconducting state, i.e. the superconducting gap $2\Delta_{\text{sc}}$. It is the minimum energy to break a Cooper pair. We estimate Δ_{sc} as the half distance between the position of the coherence peaks in $A_{\text{nor}}(\omega)$ [circles in Fig. 1(b)].

From $A_{\text{an}}(\omega)$, which for d -wave superconductivity is real and odd in frequency, we extract key features of the dynamics of the superconducting pairs, namely the frequency intervals where pairing occurs and their relative contribution to pairing. To do that, first we extract the frequency intervals where $A_{\text{an}}(\omega)$ is positive [shaded blue regions in Fig. 1(c)]. These are the frequencies that contribute to pairing processes (i.e. pair-forming). Similarly, the frequencies over which $A_{\text{an}}(\omega)$ is negative contribute

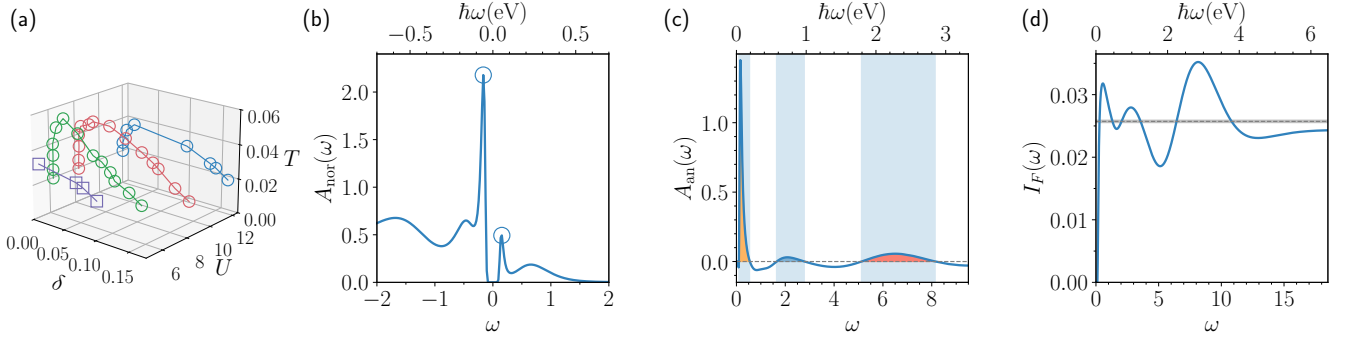


FIG. 1. (a) Superconducting transition temperature T_c^{CDMFT} versus δ for different values of U (data taken from Ref. [42]). (b) Density of states in the superconducting state $A_{\text{nor}}(\omega)$. The half distance between the position of the coherence peaks (marked by open circles) gives the superconducting gap Δ_{sc} and is analysed in Fig. 2. (c) Anomalous spectral function $A_{\text{an}}(\omega)$. The frequency regions where $A_{\text{an}}(\omega)$ is positive are those that contribute to pairing: they are shaded with blue vertical bands and are examined in Fig. 3. The areas where $A_{\text{an}}(\omega)$ is positive are colored and analysed in Fig. 4. (d) Cumulative spectral weight of the order parameter $I_F(\omega)$. Horizontal line denotes the superconducting order parameter $|\Phi|$ computed independently. Data in panels (b), (c) and (d) are for $U = 12$, $T = 1/50$ and $\delta \approx 0.02$. Frequencies are converted into physical units with $t = 350$ meV.

to depairing processes (i.e. pair-breaking). Second, we calculate the corresponding areas between $A_{\text{an}}(\omega)$ and the frequency axis [colored areas in Fig. 1(c)] to identify the relative contribution to pairing for each frequency range, as explained in the following paragraph.

To show that positive and negative anomalous spectral weight determines the frequency range where pairing and depairing arise, we can turn to the behavior of the cumulative spectral weight of the order parameter $I_F(\omega)$ [Fig. 1(d)]. In the limit $\omega \rightarrow \infty$, $I_F(\omega)$ converges to the superconducting order parameter $|\Phi|$ (horizontal grey line) [see also supplemental Fig. S6]. At low temperatures, $I_F(\omega)$ is approximately the integral of $A_{\text{an}}(\omega)$ over the positive frequencies, i.e. $I_F(\omega) \approx \int_0^\omega \frac{d\omega'}{2\pi} A_{\text{an}}(\omega')$. Hence, positive anomalous spectral weight $A_{\text{an}}(\omega)$ enhances $|\Phi|$ and thus is pair-forming, whereas negative weight depletes $|\Phi|$ and thus is pair-breaking. Hence, we can extract the pair-forming (pair-breaking) frequencies from the frequency ranges where $I_F(\omega)$ is increasing (decreasing). Similarly, we can extract the contribution to pairing (depairing) from the difference between a maximum (minimum) value of $I_F(\omega)$ and its preceding minimum (maximum) value.

Superconducting gap— Figure 2(a) shows the superconducting gap Δ_{sc} as a function of doping for different values of U . Δ_{sc} is defined as half of the energy distance between the coherence peaks in $A_{\text{nor}}(\omega)$. Physically, it reflects the pairing strength. Starting from high doping, as the doping decreases, Δ_{sc} increases. For $U > U_{\text{MIT}}$, and on decreasing doping further, Δ_{sc} flattens. Remarkably, for $U > U_{\text{MIT}}$, the doping dependence of Δ_{sc} contrasts with that of the superconducting order parameter $|\Phi|$, which first increases and then decreases as a function of doping [open squares in Fig. 4]. The value of doping for which $|\Phi|$ is maximum, $\delta_{\Phi\text{max}}$, is indicated by a filled symbol on each curve. Given that this doping is found [45] to

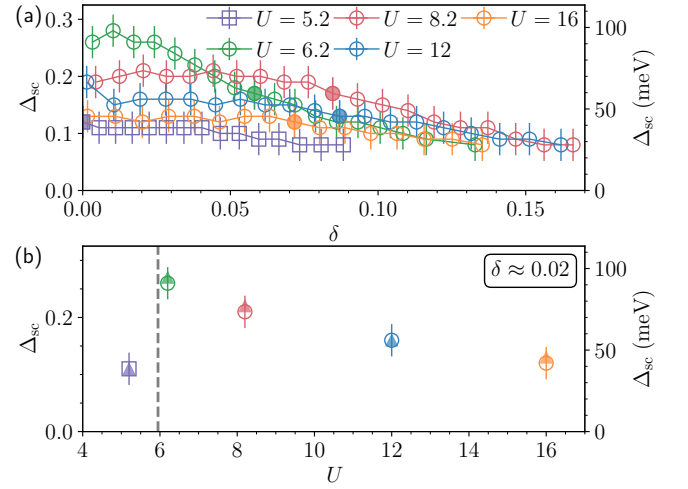


FIG. 2. (a): Superconducting gap Δ_{sc} versus δ for different values of U , as determined by the half of the frequency difference of the coherence peaks in $A_{\text{nor}}(\omega)$, see e.g. Fig. 1(b). Error bars indicate the uncertainty in determining the peaks. For each value of U , the filled symbol denotes the doping at which the superconducting order parameter $|\Phi(\delta)|$ has a maximum. (b) Δ_{sc} at fixed doping $\delta \approx 0.02$ versus U . The dashed vertical line marks the critical threshold $U_{\text{MIT}} \approx 5.95$ [47] for opening the Mott gap at half-filling. Filled up triangles denote the position of the low-frequency peak in $A_{\text{an}}(\omega)$, which tracks Δ_{sc} . Data are converted into physical units with $t = 350$ meV.

be larger than the optimal doping (i.e. the doping that maximises $T_c^{\text{CDMFT}}(\delta)$), the doping dependence of Δ_{sc} also contrasts with that of T_c^{CDMFT} . Hence, in the underdoped region for $U > U_{\text{MIT}}$, Δ_{sc} flattens while both T_c^{CDMFT} and $|\Phi|$ drop on approaching the Mott insulator at $\delta = 0$. This non-BCS behavior is compatible with previous calculations [32, 43, 48–52] and with ARPES experiments in hole-doped cuprates [53].

Figure 2(b) shows Δ_{sc} versus U at the fixed low doping

$\delta \approx 0.02$. Remarkably, $\Delta_{\text{sc}}(U)$ shows a non-monotonic behavior, peaking around the underlying normal state Mott transition at U_{MIT} (dashed vertical line). In contrast, $|\Phi|$ at this doping level decreases monotonically with increasing U .

Frequency scales where pairing arises– Next, we analyse the frequency intervals where pairing occurs. These are given by the regions where $A_{\text{an}}(\omega)$ is positive and are shown in Fig. 3 with vertical and colored bars, for several values of δ and U . Blank space between these bars indicates the regions where $A_{\text{an}}(\omega)$ is negative, i.e. where depairing occurs. Up (down) triangles mark the maxima (minima) in each frequency region.

Although $A_{\text{an}}(\omega)$ for a given value of U and δ may show a complicated behavior due to the limitations of the analytical continuation, a few trends emerge. As a function of frequency, intervals yielding pair-forming processes alternate with intervals yielding pair-breaking processes, implying that pairing arises at multiple frequency scales.

Let us consider the low-frequency scale first. (i) $A_{\text{an}}(\omega)$ has a gap between $\omega = 0$ and $\omega \approx 0.2$, mainly at small doping levels (see Fig. 5 in Appendix for a low-frequency zoom of Fig. 3). (ii) After this gap, $A_{\text{an}}(\omega)$ is positive on a narrow frequency range, which for all values of U and δ lies between $\omega \approx 0$ and $\omega \approx 0.6$. This frequency scale is of the order of $J/2$, suggesting that the long-lived pair-forming processes occurring in this frequency interval are associated with short-range spin fluctuations, as pointed out earlier [27, 28, 31]. (iii) This low-frequency region leading to pairing occurs for all doping levels and for all U , suggesting that it is unrelated to the underlying normal-state strongly correlated pseudogap, which only develops for $U > U_{\text{MIT}}$ and small dopings [54–56]. (iv) In this low-frequency region, $A_{\text{an}}(\omega)$ shows a prominent peak, whose position tracks Δ_{sc} , both as a function of U (filled up triangles vs open symbols in Fig. 2(b)) and δ (Fig. 5). As noted in Ref. [32], this suggests that Δ_{sc} is the energy scale where pairing is maximum.

Pair-forming processes also occur at higher frequency scales. The spectra for $U \gtrsim 8.2$ suggest to identify an intermediate and a high-frequency scale, although this is a simplification for more complicated spectra. The intermediate frequency region leading to pairing is visible for example at $U = 12$, where $A_{\text{an}}(\omega)$ is positive around $\omega \approx 2$ with an approximate width of 1. This intermediate frequency scale, which slightly increases with increasing U , is larger than J or Δ_{sc} and is not restricted to low doping or large values of U .

The high-frequency region leading to pairing is visible for example at $U = 12$ around $\omega \approx 6$, with an approximate width of 4. This high-frequency scale is spread over a broad frequency range and occurs for all doping levels and for all U . This frequency scale is of the order of U , suggesting that the short-lived pair-forming processes in this frequency interval are associated with the creation of a pair from an electron on a doubly occupied state and

another electron in a singly occupied state [27, 28].

Contribution to pairing– Next, we study the contribution to pairing for each frequency interval where pairing occurs. This can be estimated by the area under the positive regions of $A_{\text{an}}(\omega)$. Figure 4 shows the largest areas, divided by 2π , under the positive regions of $A_{\text{an}}(\omega)$ at low ($\mathcal{C}_{\text{low}}^+$, yellow filled circles), intermediate ($\mathcal{C}_{\text{int}}^+$, blue filled diamonds), and high frequencies ($\mathcal{C}_{\text{high}}^+$, red filled squares) versus δ for different values of U [panels (a)-(e)] and versus U at $\delta \approx 0.02$ [panel (f)].

For $U > U_{\text{MIT}}$, $\mathcal{C}_{\text{low}}^+$ has a dome-like shape versus δ and overall decreases with increasing U . Hence, a key finding is that on approaching the Mott insulator at $\delta = 0$, the drop of $|\Phi|$ and $T_{\text{c}}^{\text{CDMFT}}$ is associated with the reduction of the area of the low frequency peak of $A_{\text{an}}(\omega)$. Furthermore, both low-frequency peak position [triangles in Fig. 2(b)] and $\mathcal{C}_{\text{low}}^+$ [circles in Fig. 4(f)] have similar non-monotonic behavior versus U .

The contribution to pairing of higher frequencies is markedly different. Overall, $\mathcal{C}_{\text{int}}^+$ is small, has a mild doping dependence, and slightly increases with increasing U . For $U > U_{\text{MIT}}$, $\mathcal{C}_{\text{high}}^+$ rapidly increases with increasing U . As shown in Fig. 4(f), for $U > U_{\text{MIT}}$ the ratio $\mathcal{C}_{\text{low}}^+/\mathcal{C}_{\text{high}}^+$ decreases with increasing U , and for $U = 16$ the largest contribution to pairing comes from the high frequency pair-forming processes. The progressive importance of the higher frequencies pair-forming processes with increasing U strengthens the findings in Refs. [27, 28].

Having analysed the contribution to pairing for each frequency interval, we examine their *net* contribution to pairing. To this end, note that from Fig. 4(a)-(e), $\mathcal{C}_{\text{low}}^+(\delta)$ is greater than $|\Phi(\delta)|$ [open squares], for all values of U and δ . This is possible because $A_{\text{an}}(\omega)$ has both positive and negative spectral weight. Importantly, it means that the magnitude of the negative anomalous spectral weight at intermediate to high frequencies is overall larger than the positive one. As a result, $\mathcal{C}_{\text{int}}^+$ and $\mathcal{C}_{\text{high}}^+$ are completely canceled out and $\mathcal{C}_{\text{low}}^+$ is partly canceled out, so that only a fraction of $\mathcal{C}_{\text{low}}^+$ contributes to $|\Phi|$ and thus to pairing. Physically, this key finding means that the higher frequencies pair-forming processes are outweighed by the pair-breaking ones, so that only a fraction of the low-frequency pair-forming processes provides a net contribution to pairing. Put another way, the net contribution to pairing comes only from the low-frequency pair-forming processes.

The partial cancellation of the anomalous spectral weight can also immediately be deduced from the behavior of the cumulative spectral weight of the order parameter $I_F(\omega)$ [see e.g. Fig. 1(d)]: at low frequency, $I_F(\omega)$ overshoots $|\Phi|$. If pairing had a contribution from higher frequencies, then $|\Phi|$ would be larger than the value of the low frequency peak, $I_F(\omega_p)$. Similarly, Figs. 4(a)-(e) show that $I_F(\omega_p)$ [yellow crosses], which basically coincides with $\mathcal{C}_{\text{low}}^+$, is larger than $|\Phi|$ for all values of U and

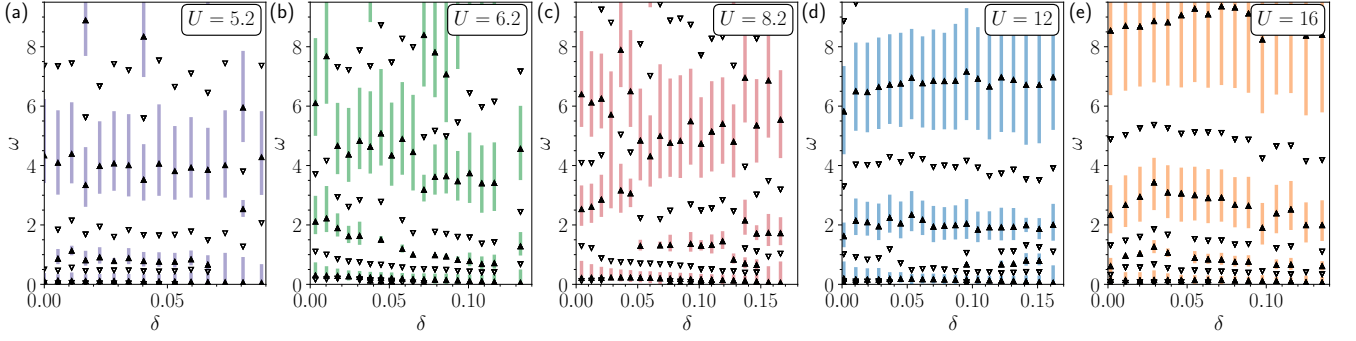


FIG. 3. Vertical bars indicate the frequency regions where $A_{\text{an}}(\omega)$ is positive, for several values of doping. Up (down) triangles denote the maxima (minima) in each frequency region. Each panel shows data for a given interaction strength U .

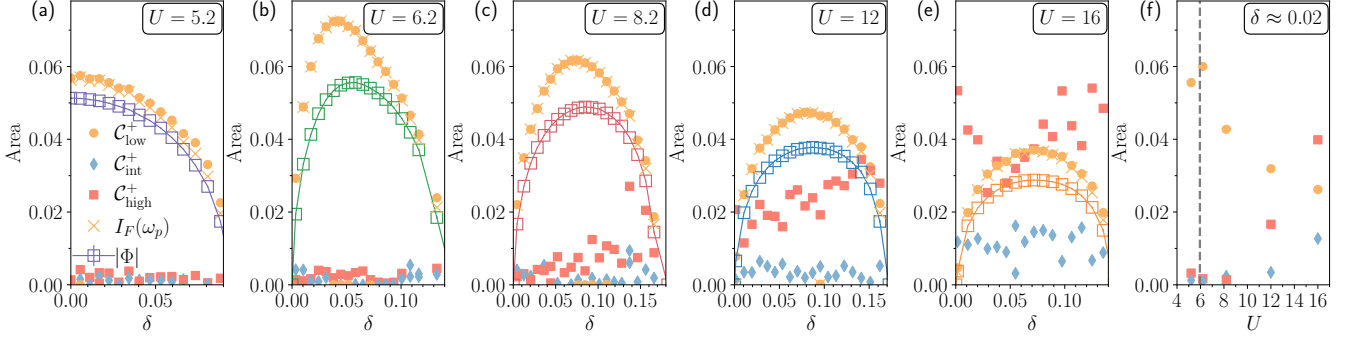


FIG. 4. The largest areas, divided by 2π , under the positive regions of $A_{\text{an}}(\omega)$: C_{low}^+ (low frequencies, yellow filled circles), C_{int}^+ (intermediate frequencies, blue filled diamonds), C_{high}^+ (high frequencies, red filled squares). They are calculated as follows. With the composite trapezoidal method, we find the four largest areas under the positive regions of $A_{\text{an}}(\omega)$ and their support $[\omega_{\text{in}}^i, \omega_{\text{fin}}^i]$, with $i = 1, \dots, 4$. If ω_{in}^i is in the $(0, 0.4]$ range, the corresponding area is C_{low}^+ . Similarly, if $\omega_{\text{in}}^i \in (0.4, 2.5]$, the area is denoted by C_{int}^+ , and if $\omega_{\text{in}}^i \in (2.5, 8.0]$, the area is denoted by C_{high}^+ . Yellow crosses indicate the value of the low-frequency peak of the cumulative spectral weight of the order parameter, $I_F(\omega_p)$. They follow C_{low}^+ . Open squares denote the superconducting order parameter $|\Phi|$. Panels (a)-(e) show the areas versus doping δ , for different values of U . Panel (f) shows the areas versus U for fixed doping $\delta \approx 0.02$. The dashed vertical line marks U_{MIT} .

δ . This implies that the negative contributions to pairing at intermediate to high frequencies outweigh their corresponding positive contributions.

Summary– We studied the dynamics of the superconducting pairs in the 2D Hubbard model for a wide range of interaction U and doping. The superconducting gap Δ_{sc} extracted from $A_{\text{nor}}(\omega)$ does not scale with the superconducting order parameter, but instead saturates upon approaching the Mott insulator. For all values of U and δ , $A_{\text{an}}(\omega)$ undergoes multiple sign changes, indicating that pair-forming processes occur at different frequency scales and at the same time they alternate with pair-breaking ones. The contribution to pairing of each frequency scale, extracted from the area under the positive regions of $A_{\text{an}}(\omega)$, behaves differently as a function of δ and U , and shows the increased importance of high-frequency pair-forming processes with increasing U . However, the higher frequency pair-forming processes are outweighed by the pair-breaking ones, so that the net contribution to pairing comes only from the low-frequency frequency pair-forming processes. Our results provide predictions

for experiments that plan to directly measure pair correlations with ARPES [15].

Acknowledgments– This work has been partially supported by the Canada First Research Excellence Fund. Simulations were performed on computers provided by the Canada Foundation for Innovation, Calcul Québec, and Digital Research Alliance of Canada.

* corresponding author: giovanni.sordi@rhul.ac.uk

- [1] M. R. Norman, The challenge of unconventional superconductivity, *Science* **332**, 196 (2011).
- [2] D. J. Scalapino, A common thread: The pairing interaction for unconventional superconductors, *Rev. Mod. Phys.* **84**, 1383 (2012).
- [3] B. Keimer, S. A. Kivelson, M. R. Norman, S. Uchida, and J. Zaanen, From quantum matter to high-temperature superconductivity in copper oxides, *Nature* **518**, 179 (2015).
- [4] E. van Heumen, E. Muhlethaler, A. B. Kuzmenko, H. Eisaki, W. Meevasana, M. Greven, and D. van der

- Marel, Optical determination of the relation between the electron-boson coupling function and the critical temperature in high- T_c cuprates, *Phys. Rev. B* **79**, 184512 (2009).
- [5] J. P. Carbotte, T. Timusk, and J. Hwang, Bosons in high-temperature superconductors: an experimental survey, *Reports on Progress in Physics* **74**, 066501 (2011).
 - [6] S. D. Conte, C. Giannetti, G. Coslovich, F. Cilento, D. Bossini, T. Abebaw, F. Banfi, G. Ferrini, H. Eisaki, M. Greven, A. Damascelli, D. van der Marel, and F. Parmigiani, Disentangling the Electronic and Phononic Glue in a High- T_c Superconductor, *Science* **335**, 1600 (2012).
 - [7] F. Cilento, S. D. Conte, G. Coslovich, F. Banfi, G. Ferrini, H. Eisaki, M. Greven, A. Damascelli, D. v. d. Marel, F. Parmigiani, and C. Giannetti, In search for the pairing glue in cuprates by non-equilibrium optical spectroscopy, *Journal of Physics: Conference Series* **449**, 012003 (2013).
 - [8] S. Dal Conte, L. Vidmar, D. Golež, M. Mierzejewski, G. Soavi, S. Peli, F. Banfi, G. Ferrini, R. Comin, B. M. Ludbrook, L. Chauviere, N. D. Zhigadlo, H. Eisaki, M. Greven, S. Lupi, A. Damascelli, D. Brida, M. Capone, J. Bonča, G. Cerullo, and C. Giannetti, Snapshots of the retarded interaction of charge carriers with ultrafast fluctuations in cuprates, *Nature Physics* **11**, 421–426 (2015).
 - [9] P. W. Anderson, Is there glue in cuprate superconductors?, *Science* **316**, 1705 (2007).
 - [10] C. Weber, K. Haule, and G. Kotliar, Strength of correlations in electron- and hole-doped cuprates, *Nature Physics* **6**, 574 (2010).
 - [11] C. Weber, C. Yee, K. Haule, and G. Kotliar, Scaling of the transition temperature of hole-doped cuprate superconductors with the charge-transfer energy, *Europhysics Letters* **100**, 37001 (2012).
 - [12] S. Acharya, C. Weber, E. Plekhanov, D. Pashov, A. Taraphder, and M. Van Schilfgaarde, Metal-Insulator Transition in Copper Oxides Induced by Apex Displacements, *Phys. Rev. X* **8**, 021038 (2018).
 - [13] B. Bacq-Labreuil, B. Lacasse, A.-M. S. Tremblay, D. Sénéchal, and K. Haule, Toward an Ab Initio Theory of High-Temperature Superconductors: A Study of Multilayer Cuprates, *Phys. Rev. X* **15**, 021071 (2025).
 - [14] Z.-H. Cui, J. Yang, J. Tölle, H.-Z. Ye, S. Yuan, H. Zhai, G. Park, R. Kim, X. Zhang, L. Lin, T. C. Berkelbach, and G. K.-L. Chan, Ab initio quantum many-body description of superconducting trends in the cuprates, *Nature Communications* **16**, 1845 (2025).
 - [15] A. F. Kemper, F. Goto, H. A. Labib, N. Gauthier, E. H. da Silva Neto, and F. Boschini, *Observing two-electron interactions with correlation-ARPES* (2025), arXiv:2505.01504 [cond-mat.str-el].
 - [16] C. Stahl and M. Eckstein, Noise correlations in time- and angle-resolved photoemission spectroscopy, *Phys. Rev. B* **99**, 241111 (2019).
 - [17] T. P. Devereaux, M. Claassen, X.-X. Huang, M. Zaletel, J. E. Moore, D. Morr, F. Mahmood, P. Abbamonte, and Z.-X. Shen, Angle-resolved pair photoemission theory for correlated electrons, *Phys. Rev. B* **108**, 165134 (2023).
 - [18] F. Boschini, M. Zonno, and A. Damascelli, Time-resolved arpes studies of quantum materials, *Rev. Mod. Phys.* **96**, 015003 (2024).
 - [19] P. W. Anderson, The resonating valence bond state in La_2CuO_4 and superconductivity, *Science* **235**, 1196 (1987).
 - [20] A.-M. S. Tremblay, Strongly correlated superconductivity, in *Emergent Phenomena in Correlated Matter Modeling and Simulation*, Vol. 3, edited by E. Pavarini, E. Koch, and U. Schollwöck (Verlag des Forschungszentrum, Jülich, 2013) Chap. 10.
 - [21] G. Kotliar and J. Liu, Superexchange mechanism and d-wave superconductivity, *Phys. Rev. B* **38**, 5142 (1988).
 - [22] T. Maier, M. Jarrell, T. Pruschke, and M. H. Hettler, Quantum cluster theories, *Rev. Mod. Phys.* **77**, 1027 (2005).
 - [23] A.-M. S. Tremblay, B. Kyung, and D. Sénéchal, Pseudogap and high-temperature superconductivity from weak to strong coupling. Towards a quantitative theory, *Low Temp. Phys.* **32**, 424 (2006).
 - [24] M. Qin, T. Schäfer, S. Andergassen, P. Corboz, and E. Gull, The Hubbard Model: A Computational Perspective, *Annual Review of Condensed Matter Physics* **13**, 275 (2022).
 - [25] G. Kotliar, S. Y. Savrasov, K. Haule, V. S. Oudovenko, O. Parcollet, and C. A. Marianetti, Electronic structure calculations with dynamical mean-field theory, *Rev. Mod. Phys.* **78**, 865 (2006).
 - [26] A. Georges, G. Kotliar, W. Krauth, and M. J. Rozenberg, Dynamical mean-field theory of strongly correlated fermion systems and the limit of infinite dimensions, *Rev. Mod. Phys.* **68**, 13 (1996).
 - [27] T. A. Maier, D. Poilblanc, and D. J. Scalapino, Dynamics of the Pairing Interaction in the Hubbard and t - J Models of High-Temperature Superconductors, *Phys. Rev. Lett.* **100**, 237001 (2008).
 - [28] B. Kyung, D. Sénéchal, and A.-M. S. Tremblay, Pairing dynamics in strongly correlated superconductivity, *Physical Review B (Condensed Matter and Materials Physics)* **80**, 205109 (2009).
 - [29] M. Civelli, Evolution of the dynamical pairing across the phase diagram of a strongly correlated high-temperature superconductor, *Phys. Rev. Lett.* **103**, 136402 (2009).
 - [30] D. Sénéchal, A. G. R. Day, V. Bouliane, and A.-M. S. Tremblay, Resilience of d -wave superconductivity to nearest-neighbor repulsion, *Phys. Rev. B* **87**, 075123 (2013).
 - [31] E. Gull and A. J. Millis, Pairing glue in the two-dimensional Hubbard model, *Phys. Rev. B* **90**, 041110 (2014).
 - [32] A. Reymbaut, M. Charlebois, M. F. Asiani, L. Fratino, P. Sémon, G. Sordi, and A.-M. S. Tremblay, Antagonistic effects of nearest-neighbor repulsion on the superconducting pairing dynamics in the doped Mott insulator regime, *Phys. Rev. B* **94**, 155146 (2016).
 - [33] X. Dong, L. Del Re, A. Toschi, and E. Gull, Mechanism of superconductivity in the Hubbard model at intermediate interaction strength, *Proceedings of the National Academy of Science* **119**, e2205048119 (2022).
 - [34] X. Dong, E. Gull, and A. J. Millis, Quantifying the role of antiferromagnetic fluctuations in the superconductivity of the doped Hubbard model, *Nature Physics* **18**, 1293 (2022).
 - [35] K. Haule, Quantum Monte Carlo impurity solver for cluster dynamical mean-field theory and electronic structure calculations with adjustable cluster base, *Phys. Rev. B* **75**, 155113 (2007).
 - [36] P. Werner, A. Comanac, L. de Medici, M. Troyer, and A. J. Millis, Continuous-time solver for quantum impu-

- rity models, *Phys. Rev. Lett.* **97**, 076405 (2006).
- [37] E. Gull, A. J. Millis, A. I. Lichtenstein, A. N. Rubtsov, M. Troyer, and P. Werner, Continuous-time Monte Carlo methods for quantum impurity models, *Rev. Mod. Phys.* **83**, 349 (2011).
- [38] P. Sémon, C.-H. Yee, K. Haule, and A.-M. S. Tremblay, Lazy skip-lists: An algorithm for fast hybridization-expansion quantum Monte Carlo, *Phys. Rev. B* **90**, 075149 (2014).
- [39] P. Sémon, G. Sordi, and A.-M. S. Tremblay, Ergodicity of the hybridization-expansion Monte Carlo algorithm for broken-symmetry states, *Phys. Rev. B* **89**, 165113 (2014).
- [40] D. Bergeron and A.-M. S. Tremblay, Algorithms for optimized maximum entropy and diagnostic tools for analytic continuation, *Phys. Rev. E* **94**, 023303 (2016).
- [41] A. Reymbaut, D. Bergeron, and A.-M. S. Tremblay, Maximum entropy analytic continuation for spectral functions with nonpositive spectral weight, *Phys. Rev. B* **92**, 060509 (2015).
- [42] C. Walsh, M. Charlebois, P. Sémon, G. Sordi, and A.-M. S. Tremblay, Information-theoretic measures of superconductivity in a two-dimensional doped Mott insulator, *Proceedings of the National Academy of Sciences* **118**, e2104114118 (2021).
- [43] K. Haule and G. Kotliar, Strongly correlated superconductivity: A plaquette dynamical mean-field theory study, *Phys. Rev. B* **76**, 104509 (2007).
- [44] G. Sordi, P. Sémon, K. Haule, and A.-M. S. Tremblay, Strong Coupling Superconductivity, Pseudogap, and Mott Transition, *Phys. Rev. Lett.* **108**, 216401 (2012).
- [45] L. Fratino, P. Sémon, G. Sordi, and A.-M. S. Tremblay, An organizing principle for two-dimensional strongly correlated superconductivity, *Sci. Rep.* **6**, 22715 (2016).
- [46] This neglects Kosterlitz-Thouless physics.
- [47] C. Walsh, P. Sémon, D. Poulin, G. Sordi, and A.-M. S. Tremblay, Thermodynamic and information-theoretic description of the Mott transition in the two-dimensional Hubbard model, *Phys. Rev. B* **99**, 075122 (2019).
- [48] A. Paramekanti, M. Randeria, and N. Trivedi, High- T_c superconductors: A variational theory of the superconducting state, *Phys. Rev. B* **70**, 054504 (2004).
- [49] S. S. Kancharla, B. Kyung, D. Sénéchal, M. Civelli, M. Capone, G. Kotliar, and A.-M. S. Tremblay, Anomalous superconductivity and its competition with antiferromagnetism in doped Mott insulators, *Phys. Rev. B* **77**, 184516 (2008).
- [50] M. Civelli, M. Capone, A. Georges, K. Haule, O. Parcollet, T. D. Stanescu, and G. Kotliar, Nodal-Antinodal Dichotomy and the Two Gaps of a Superconducting Doped Mott Insulator, *Phys. Rev. Lett.* **100**, 046402 (2008).
- [51] E. Gull, O. Parcollet, and A. J. Millis, Superconductivity and the Pseudogap in the Two-Dimensional Hubbard Model, *Phys. Rev. Lett.* **110**, 216405 (2013).
- [52] C. Walsh, M. Charlebois, P. Sémon, A.-M. S. Tremblay, and G. Sordi, Superconductivity in the two-dimensional Hubbard model with cellular dynamical mean-field theory: A quantum impurity model analysis, *Phys. Rev. B* **108**, 075163 (2023).
- [53] J. A. Sobota, Y. He, and Z.-X. Shen, Angle-resolved photoemission studies of quantum materials, *Rev. Mod. Phys.* **93**, 025006 (2021).
- [54] G. Sordi, K. Haule, and A.-M. S. Tremblay, Finite Doping Signatures of the Mott Transition in the Two-Dimensional Hubbard Model, *Phys. Rev. Lett.* **104**, 226402 (2010).
- [55] G. Sordi, K. Haule, and A.-M. S. Tremblay, Mott physics and first-order transition between two metals in the normal-state phase diagram of the two-dimensional Hubbard model, *Phys. Rev. B* **84**, 075161 (2011).
- [56] G. Sordi, P. Sémon, K. Haule, and A.-M. S. Tremblay, Pseudogap temperature as a Widom line in doped Mott insulators, *Sci. Rep.* **2**, 547 (2012).

Appendix

Figure 5 shows a zoom in of Fig. 3 on the low frequencies.

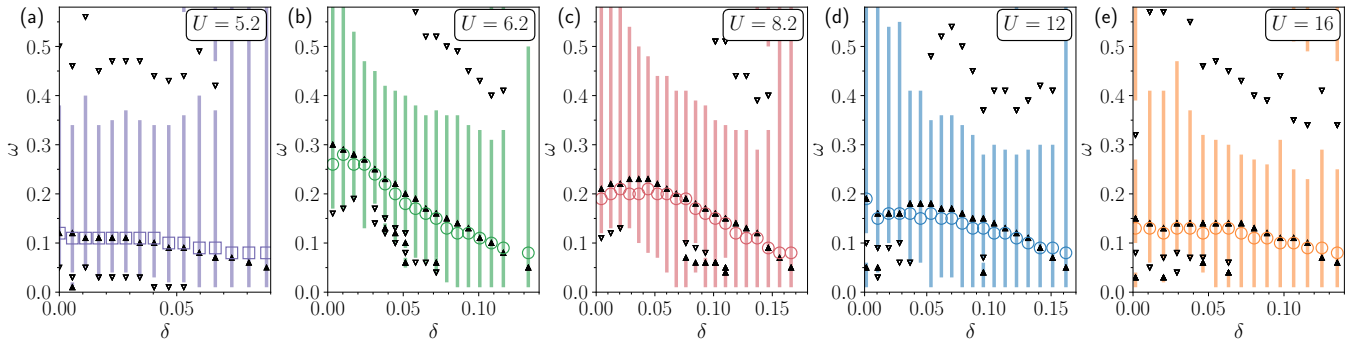


FIG. 5. Low-frequency zoom of Fig. 3. For each value of δ and U , the frequency position of the low-frequency maximum of $A_{\text{an}}(\omega)$ (filled up triangles) tracks the size of the superconducting gap Δ_{sc} (open circles), suggesting that Δ_{sc} is the energy scale where pairing is maximum [32].

Supplemental Material

$A_{\text{nor}}(\omega)$, $A_{\text{an}}(\omega)$, and $I_F(\omega)$

With the same notation of Fig. 1 of the main text, we show in Figs. S1 - S5 the density of states in the superconducting state $A_{\text{nor}}(\omega)$, the anomalous spectral function $A_{\text{an}}(\omega)$, and the cumulative spectral weight of the order parameter $I_F(\omega)$, for different values of U and doping levels δ . The color code for each value of U is the same as in the main text.

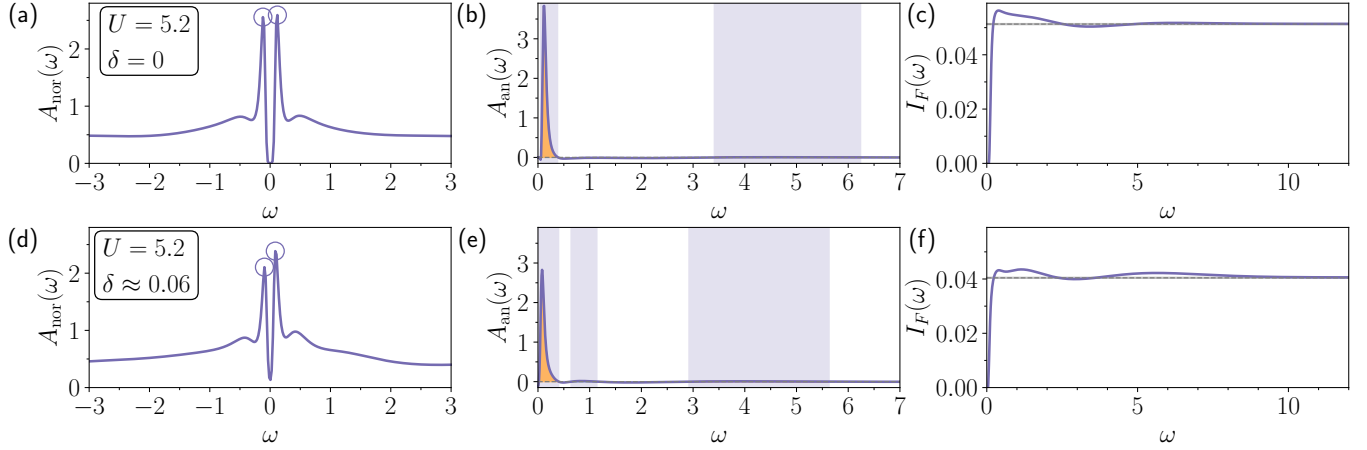


FIG. S1. (a, d) Density of states in the superconducting state $A_{\text{nor}}(\omega)$. The open circles mark the superconducting coherence peaks. (b, e) Anomalous spectral function $A_{\text{an}}(\omega)$. The frequency regions where $A_{\text{an}}(\omega)$ is positive are marked by colored vertical bands and the corresponding positive areas are colored. (c, f) Cumulative spectral weight of the order parameter $I_F(\omega)$. Horizontal line indicates the superconducting order parameter $|\Phi|$ calculated independently and directly within the impurity solver. Data are for $U = 5.2$, $T = 1/50$ and $\delta = 0$ (top row) and $\delta \approx 0.06$ (bottom row).

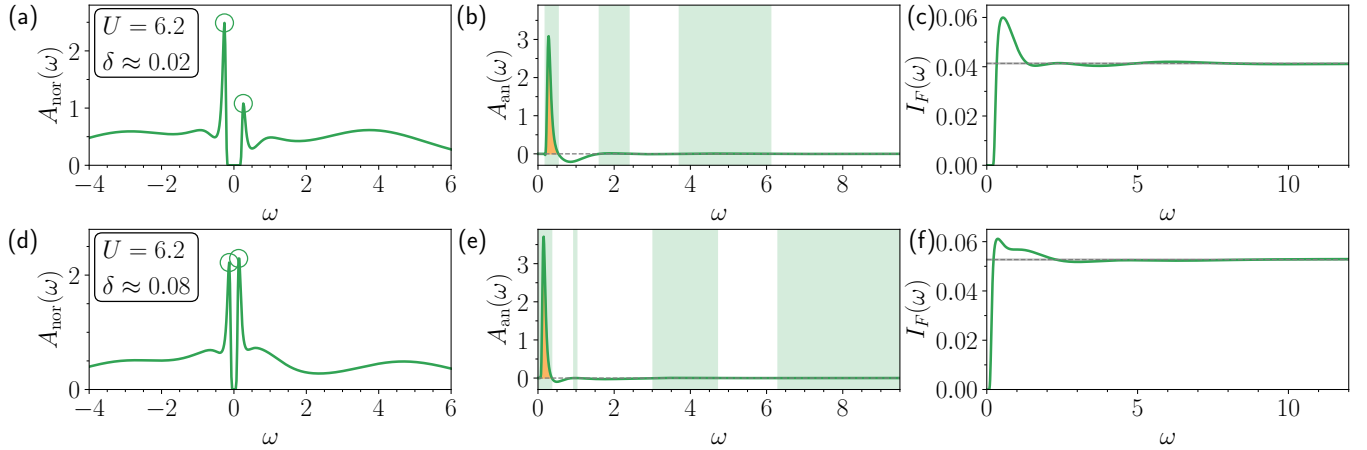


FIG. S2. Same as Fig. S1, but for $U = 6.2$, $T = 1/50$ and $\delta \approx 0.02$ (top row) and $\delta \approx 0.08$ (bottom row).

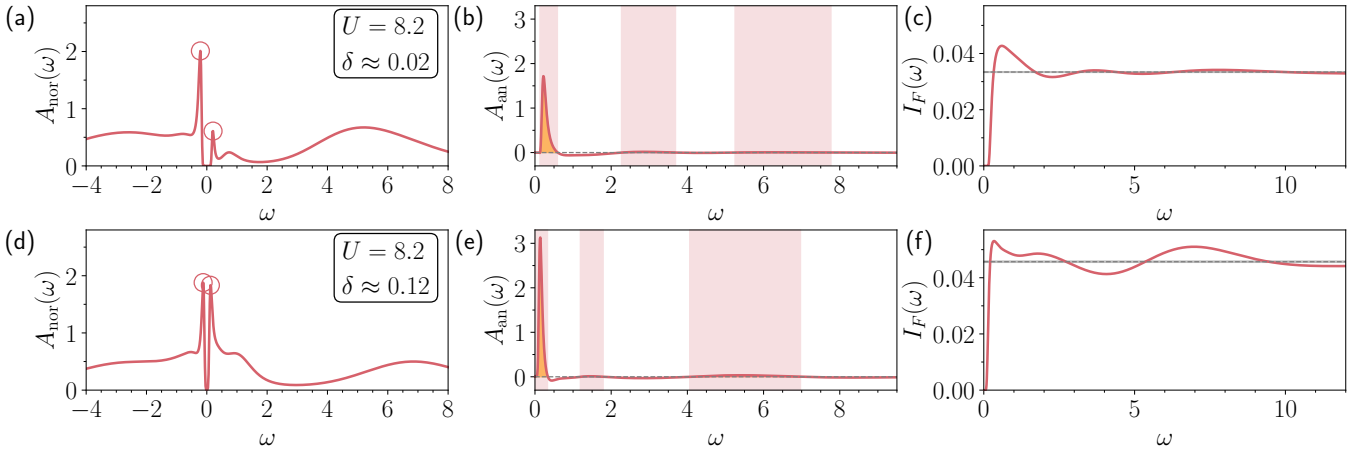


FIG. S3. Same as Fig. S1, but for $U = 8.2$, $T = 1/50$ and $\delta \approx 0.02$ (top row) and $\delta \approx 0.12$ (bottom row).

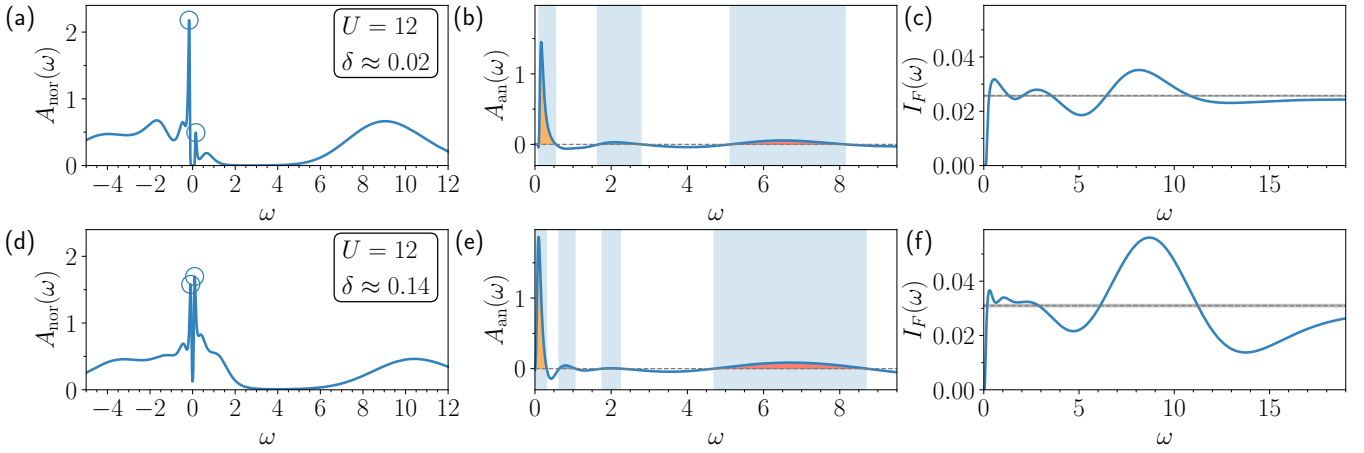


FIG. S4. Same as Fig. S1, but for $U = 12$, $T = 1/50$ and $\delta \approx 0.02$ (top row) and $\delta \approx 0.14$ (bottom row).

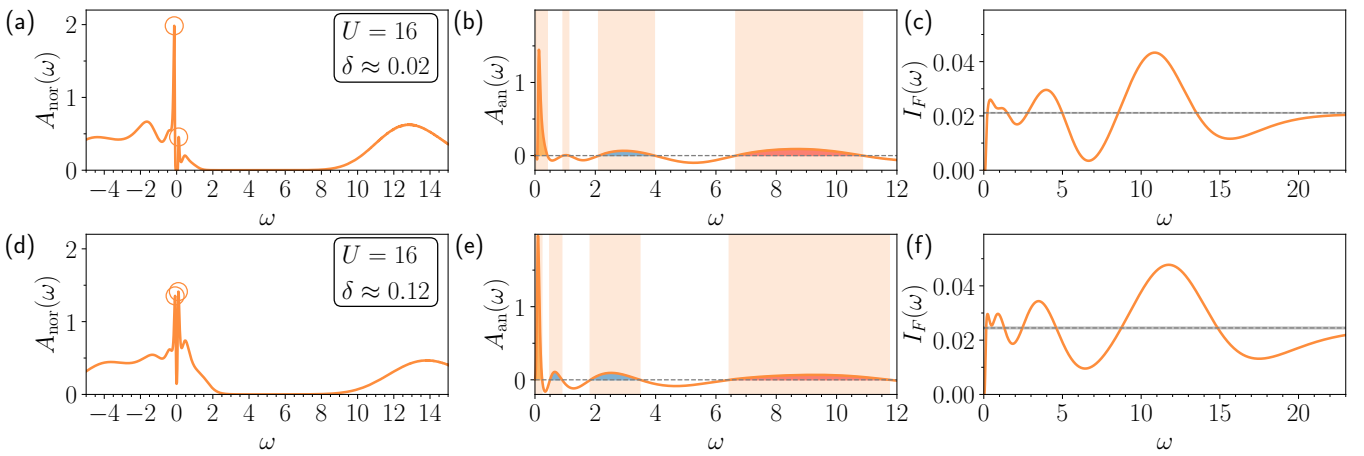


FIG. S5. Same as Fig. S1, but for $U = 16$, $T = 1/50$ and $\delta \approx 0.02$ (top row) and $\delta \approx 0.12$ (bottom row).

Superconducting order parameter

In the limit $\omega \rightarrow \infty$, the cumulative spectral weight of the order parameter $I_F(\omega)$ converges to the superconducting order parameter $|\Phi|$. This provides a consistency check for the analytically continued anomalous spectral function $A_{\text{an}}(\omega)$. Figure S6 shows $|\Phi|$ as a function of doping δ and for different values of U , computed in two independent ways: (i) within the impurity solver (open squares) and (ii) from $\lim_{\omega \rightarrow \infty} I_F(\omega)$ (filled circles). The overall good agreement between the two methods indicates that the main features of $A_{\text{an}}(\omega)$ are correctly captured by the analytical continuation.

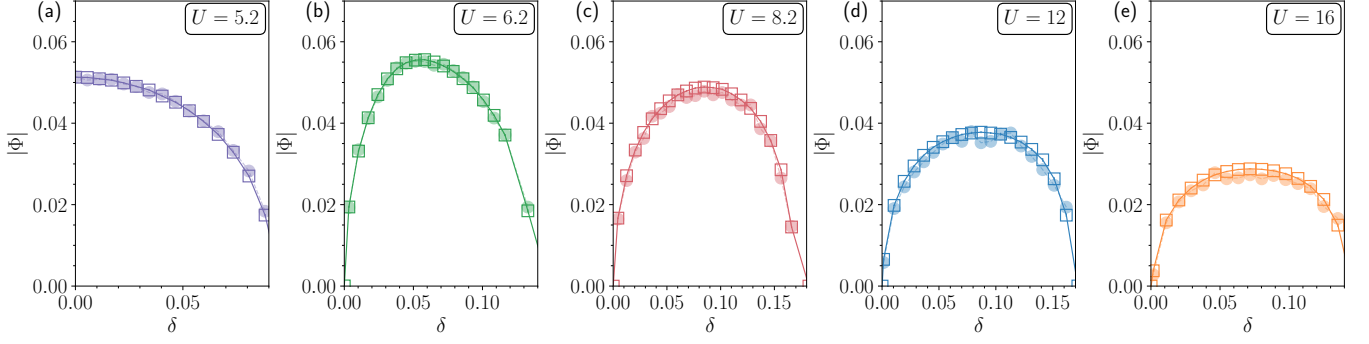


FIG. S6. Superconducting order parameter $|\Phi|$ at $T = 1/50$ as a function of doping δ and for different values of U , computed in two independent ways: (i) directly within the impurity solver, from $\Phi = \langle F_{\mathbf{K}=(\pi,0)}(\tau = 0^+) \rangle$ (open squares) and (ii) from $\lim_{\omega \rightarrow \infty} I_F(\omega)$ (filled circles). The latter has been estimated as the average over the frequency range $\omega \in [30, 40]$ of $I_F(\omega)$.